JOURNAL OF AIRCRAFT
Vol. 29, No. 3, May–June 1992

Wake Effects on the Prediction of Transonic Viscous Flows Around Airfoils

D. P. Coiro,* P. de Matteis,† and M. Amato†
CIRA, Centro Italiano Ricerche Aerospaziali, Capua-(CE), Italy

A semi-inverse viscous/inviscid coupling technique for the calculations of compressible airfoil flows is presented. The Euler equations in integral form are solved in the inviscid part and the integral compressible boundary-layer equations in inverse form are solved in the viscous part. Both displacement and curvature effects have been included in the wake computation. Interaction is realized using the equivalent sources method. This technique has been applied to the calculation of the aerodynamic characteristics of airfoils both in subsonic and transonic regimes. It has been shown that the contributions of body displacement, wake displacement, and wake curvature effects are particularly important in the evaluation of the aerodynamic coefficients, especially drag. Different ways of computing the equivalent sources fluxes in the wake and the influence of the fixed-wake dividing streamline shape have been investigated and are discussed.

Nomenclature

C_d = drag coefficient
C_f = skin-friction coefficient
C_l = lift coefficient
C_p = pressure coefficient
Dstar = displacement thickness
E = total energy
f, g = flux vectors, defined by Eqs. (2)
H = total enthalpy or boundary-layer shape factor
K = curvature
M = Mach number
p = static pressure
$Q(W)$ = net flux out of the cell
Re = Reynolds number
s, n = boundary-layer coordinates
U_e = velocity at the edge of boundary layer
U, V = Cartesian components of velocity
u, v = components of velocity in boundary-layer coordinates
Vol = cell volume
W = field variables vector
x, y = Cartesian coordinates
α = angle of attack
β = wake centerline angle
γ = specific heat ratio
Δ = jump across the wake centerline
δ^* = boundary-layer displacement thickness
$\partial\Omega$ = control-volume boundary
ε = convergence parameter
θ = boundary-layer momentum thickness
ρ = density
Ω = control volume
ω = relaxation factor

Superscripts
n = iteration step
T = tensor transposition index
$\sim$ = external velocity from boundary-layer calculation

Subscripts
∞ = infinity or freestream
e = boundary-layer edge
t = time
u, l = upper, lower
w = wall

Introduction

NUMERICAL algorithms for the prediction of viscous effects on the aerodynamic characteristics of airfoils can be divided in two categories: global procedures that solve a viscous model throughout the whole domain and interactive procedures that couple viscous and inviscid solutions. With the advent of supercomputers and superminicomputers, the numerical solution of the Navier-Stokes equations, or an appropriate approximation of them, is becoming more routine. The large running time even on supercomputers and the memory requirements are such, however, that it is not yet possible to employ this approach in a design environment. Moreover, it is not yet possible to employ grids with high enough resolution to capture the small length scales present in a turbulent boundary layer. The interactive approach takes advantage of the physics of the flow, dividing the computational field in domains in which different models can be applied. The most popular model based on this concept couples the boundary layer to an appropriate inviscid model. Despite the increased complexity of treating multiple solution algorithms and domain interfaces, interactive procedures are more cost effective than global ones. A comprehensive review of interactive procedures for both airfoil and wing analyses can be found in Ref. 1.

In transonic flows, the boundary layer strongly affects the pressure distribution. In fact, the boundary layer on the body weakens the inviscid shock wave driving it upstream, whereas the wake reduces the pressure at and near the trailing edge with respect to the values obtained neglecting its contributions. Furthermore, shocks thicken the boundary layer, frequently inducing flow separation and increasing the viscous influence on the global aerodynamic characteristics. Viscous/inviscid interaction procedures based on the full-potential inviscid equation have been widely investigated and are routinely used as an aerodynamic design tool.[2] The solutions obtained with these schemes are satisfactory if shocks are weak. When shocks are strong, the vorticity downstream becomes significant, and it is difficult to conserve both mass and momentum across the shock, giving rise to spurious productions and then spurious sink drag. Furthermore, looking to three-dimensional applications, the full-potential model cannot take into account the vortex flow near the wing tip.

Presented as Paper 90-3061 at the AIAA 8th Applied Aerodynamics Conference, Portland, OR, Aug. 20–22, 1990; received Nov. 29, 1990; revision received April 22, 1991; accepted for publication April 22, 1991.

*Senior Researcher; currently Research Scientist, Istituto di Progetto Velivoli, Università degli Studi di Napoli, via Claudio 21, 80125 Napoli, Italy. Member AIAA.

†Junior Researcher, Via Maiorise, 81043 Capua (CE), Italy. Member AIAA.

Therefore, viscous/inviscid interaction procedures based on the Euler equations seems to be of more general applicability.[3] To the authors' knowledge, however, few papers have put in evidence the yet unsolved problem of numerical drag prediction.

The present work investigates the main factors that influence the computation of the global aerodynamic coefficients, with particular regard to drag. A viscous/inviscid coupling technique, previously developed for the calculation of the aerodynamic characteristics of simple and multielement airfoils,[4] has been improved by the inclusion of the wake computation. Both wake displacement and curvature effects have been included for single-airfoil flow computations. The boundary-layer equations are solved using an integral method, which is particularly advantageous because accuracy comparable to that of finite difference methods is obtained at a much lower computational cost.

Viscous/inviscid coupling is realized through the use of the blowing approach, first proposed by Lighthill.[5] In this way, the same grid can be used for the inviscid solution during the iteration procedure. Simulation of viscous effects is realized by means of an equivalent distribution of sources on the body and by a source/vortex distribution in the wake. While the matching conditions in the wake region are usually given in terms of tangential and normal velocity on the dividing streamline, in the discretization of the Euler equations fluxes must be computed. In this paper, two ways of computing fluxes related to source and vortex distributions in the wake region are presented and compared numerically.

The geometry of the wake dividing streamline is a further unknown of the problem. In the present work, this geometry is maintained fixed during the iteration process and coincides with the trailing-edge grid line. Such an approach is very advantageous because of the low additional computational costs required for the wake calculations. An appropriate choice of the dividing streamline shape, however, is necessary to get physically consistent results. Results obtained using different wake shapes have been analyzed and compared.

Numerical investigations have been performed to compare the influence on the solution of three viscous contributions: body displacement, wake displacement, and wake curvature. Results are presented for single-element airfoils in subcritical and supercritical flow conditions. Attention has been devoted to the influence of the wake on the aerodynamic forces. It is shown that the wake calculation inclusion is particularly important for drag prediction.

Inviscid Method

The unsteady Euler equations written in integral form are

$$\frac{\partial}{\partial t}\iint_{\Omega} W\,dx\,dy + \int_{\partial\Omega}(f\,dy - g\,dx) = 0 \qquad (1)$$

In a two-dimensional Cartesian reference system, this equation can be expressed as

$$\begin{aligned} W &= [\rho, \rho U, \rho V, \rho E]^T \\ f &= [\rho U, \rho U^2 + p, \rho UV, \rho HU]^T \\ g &= [\rho V, \rho VU, \rho V^2 + p, \rho HV]^T \end{aligned} \qquad (2)$$

For a perfect gas the following relationship holds:

$$H = \frac{p}{(\gamma - 1)\rho} + \frac{1}{2}(U^2 + V^2) \qquad (3)$$

These equations are solved numericaly using the finite-volume scheme developed by Jameson et al.[6]

The following set of ordinary differential equations is obtained if Eq. (1) is applied to each cell of the grid, storing in its center the mean value of W:

$$\frac{d}{dt}(Vol\ W) + Q(W) = 0 \qquad (4)$$

where $Q(W)$ is approximated by evaluating the flux through each face as the average of its values in the center of the adjacent cells. The resulting system of equations is integrated in time using a fourth-order Runge-Kutta scheme with five stages. Artificial dissipation terms are composed of a blend of second and fourth differences with adaptive coefficients, to eliminate the frequency modes of the residual. Different techniques for convergence acceleration have been used, the most effective being full multigrid.[7]

Far-field boundary conditions are imposed applying local one-dimensional characteristics theory and taking into account the velocity induced by the vortex schematization of the lifting body. At the wall, the boundary condition corresponds to the specified mass flux. For inviscid calculations, zero convective flux is imposed and the pressure is evaluated by extrapolating the cell center value using the normal component of the momentum equation.[8]

Viscous Method

The viscous flow calculation method is based on the solution of the integral compresssible turbulent boundary-layer equations, written both in direct and inverse form.[9] The method is based on the solution of the momentum and mean-flow turbulent kinetic energy integral equations.[10] A fourth-order four-stage explicit Runge-Kutta scheme is used to solve the direct and/or inverse system of equations. A pointwise control of the integration step is introduced in the calculations to avoid numerical instabilities. A distinguishing feature of the direct and inverse integral methods is the way in which the dissipation integral is evaluated, as explained in Ref. 11. Green's method[12] has also been coded, both in direct and in inverse form.[9] In this method, the auxiliary equations to the momentum are represented by the entrainment and the lag-entrainment equations.

Laminar boundary layers are solved using the compressible version of Thwaites's method. The transition point location can be either calculated or prescribed. The starting value of the shape factor H is evaluated using a correlation law based on the local equilibrium hypothesis. Even if this value does not affect the boundary-layer solution too much, far from equilibrium it has to be carefully evaluated to avoid numerical instability.

Wake Computation

To compute the wake flow, the dividing streamline approach is followed.[13] Two separate boundary layers are solved for the upper and lower halves, setting to zero the skin-friction coefficient in the boundary-layer equations. A problem that arises when considering this approach is that the position of the dividing streamline is not known a priori but should be found during the calculation. For computational saving and simplicity, one useful approximation consists in keeping the dividing streamline fixed during iterations and aligned with the grid starting at the trailing edge of the airfoil. The trailing-edge grid line may be neither part of a grid generated in some way or a potential streamline previously calculated. The shape of the dividing streamline changes the integration path of the boundary layer and the physical placement of the source/vortex sheet employed to build up the equivalent inviscid flow. It should be remarked, however, that the main influence comes from the portion of the wake nearest the trailing edge. The second-order terms in the boundary-layer equations due to the streamline curvature are neglected on both the body and wake. Curvature viscous effects due to the presence of the wake are considered in the equivalent inviscid flow by suitable matching conditions described later.

Grid Generation

To analyze the influence of the dividing streamline shape, here considered fixed and aligned with the trailing-edge grid line, two grid-generation schemes have been employed to

generate different O-type structured meshes. Our scheme is the unusual conformal mapping used by Jameson et al.,[6] in which the trailing-edge grid line has any shape that will preserve the quality of the global grid. In the second generation procedure, the trailing-edge grid line coincides with the trailing-edge streamline generated by a panel method. The desired number of points is then distributed with a prescribed stretching on the streamline by a one-dimensional elliptic scheme. This is considered a fixed boundary of the computational domain. The discretization is realized again by an elliptic scheme.[14] Grid spacing and orthogonality at the body and outer boundary can be controlled. Furthermore, orthogonality can be imposed between the selected trailing-edge potential streamline and the intersecting grid lines, maintaining in this way the smoothness of the grid. Figure 1 shows the trailing-edge generated by conformal mapping and the potential streamline in the region close to the trailing edge.

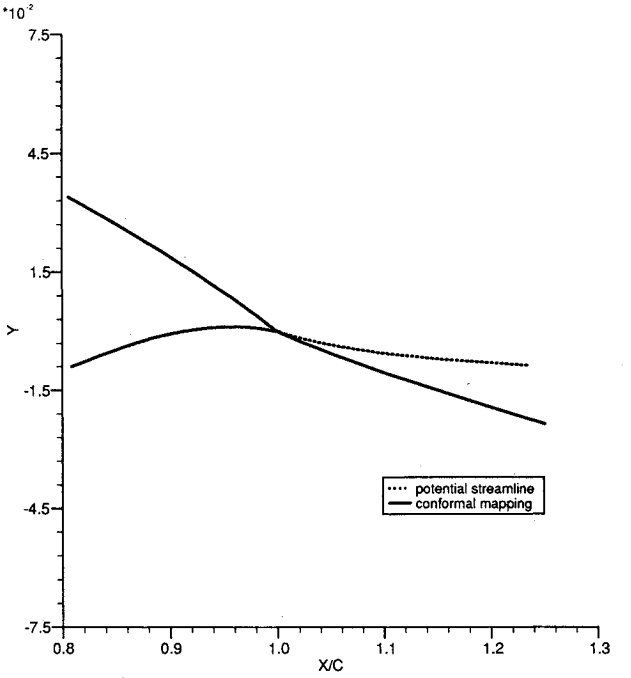

Fig. 1 Comparison between selected wake dividing line geometries for the RAE 2822 airfoil.

Viscous/Inviscid Interaction

Viscous/inviscid interaction is an iterative process during which an equivalent inviscid solution is built up by coupling the external inviscid flow to the boundary layer. One way to proceed is to thicken the body by an amount corresponding to the displacement thickness. Alternatively, the geometry is left unchanged while modifying the boundary conditions on the body and on the wake through the imposition of a transpiration velocity. The equivalence of the two approaches has been demonstrated analytically by Lighthill.[5] The blowing approach is the most suitable for coupling the boundary layer with an Euler solver because the computational grid remains fixed during the iteration.

Body Matching Conditions

Unlike a potential flow/boundary-layer interaction method, an Euler/boundary-layer approach using the equivalent sources concept requires additional information to be specified for the equations of momentum and energy. The derivation of the expressions for the fluxes due to the wall transpiration can be found in Ref. 15. Only the final expressions are reported here:

$$\begin{aligned} \rho_e v &= \frac{\mathrm{d}}{\mathrm{d}s}[\rho_e U_e \delta^*] \\ \rho_e U v &= U \frac{\mathrm{d}}{\mathrm{d}s}[\rho_e U_e \delta^*] \\ \rho_e V v &= V \frac{\mathrm{d}}{\mathrm{d}s}[\rho_e U_e \delta^*] \\ \rho H v &= H \frac{\mathrm{d}}{\mathrm{d}s}[\rho_e U_e \delta^*] \end{aligned} \tag{5}$$

The pressure at the wall is determined by the normal momentum relation derived by Rizzi[8] under the hypothesis of impermeable surface. Thomas[16] has subsequently shown that the inclusion in the normal momentum relation of permeability effects due to the presence of the boundary layer does not affect significantly wall pressure extrapolation. Thus, the original formulation of Rizzi has been maintained.

Wake Matching Conditions

In deriving the expressions (5), only the condition $v_w = 0$ is required; no assumption needs to be made for u_w. If we suppose to perform the wake calculations on the dividing streamline of the wake in the real viscous flow, the condition $v_w = 0$ is still satisfied along it.[1] Thus, the same expression for the transpiration velocity derived for the body can be used both for the upper and lower sides of the wake. Therefore, the following expression results:

$$(v)_{u,l} = \left[\frac{1}{\rho_e}\frac{\mathrm{d}}{\mathrm{d}s}(\rho_e U_e \delta^*)\right]_{u,l} \tag{6}$$

It must be emphasized that the line along which the wake calculations are performed is a branch cut in the computational domain of the equivalent inviscid flow. Two different approaches have been followed to evaluate the matching conditions on the wake line. In the first, the fluxes (5) are evaluated on the upper and lower sides separately and then their sum is considered in the balance of the faced cells. In the second approach, the normal velocity jump is computed first; then this is used to evaluate the fluxes for the upper and lower faced cells. In this case, the following expressions result:

$$\begin{aligned} (\text{mass})_{u,l} &= \rho_{u,l}\Delta v \\ (\text{momentum } x)_{u,l} &= (\rho U)_{u,l}\Delta v \\ (\text{momentum } y)_{u,l} &= (\rho V)_{u,l}\Delta v \\ (\text{energy})_{u,l} &= (\rho H)_{u,l}\Delta v \end{aligned} \tag{7}$$

The Cartesian velocity components are given by

$$\begin{aligned} U_{u,l} &= (U_e \cos\beta)_{u,l} - \Delta v(\sin\beta)_{u,l} \\ V_{u,l} &= (U_e \sin\beta)_{u,l} + \Delta v(\cos\beta)_{u,l} \end{aligned} \tag{8}$$

Here, $\sin\beta$ and $\cos\beta$ are the Cartesian components of the vector tangent to the wake line. Both approaches have been tested, and only minor differences occurred.

Curvature Effects

Although the curvature terms in the boundary-layer equations are of second order in magnitude, the effect of wake curvature inclusion can be significant on the equivalent inviscid solution. In fact, these effects are simulated by pressure discontinuities on the dividing streamline. Assembling the validity of the boundary-layer equations in each half of the wake and considering the curvature costant across the viscous layer, the following expression for the pressure jump can be derived in terms of the integral relations

$$\Delta p = [K^* \rho_e U_e^2(\delta^* + \theta)]_u + [K^* \rho_e U_e^2(\delta^* + \theta)]_l \tag{9}$$

where $K^* = K_w + (\mathrm{d}^2/\mathrm{d}s^2)\delta^*$, with K_w equal to the wall curvature.[1,13] The curvature is assumed positive for a convex surface. The pressure discontinuity can be related to a tangential velocity jump through the Bernoulli incompressible

equation, and then the wake curvature effects can be simulated by a vortex sheet. The following velocity jump can be found:

$$\Delta u = -\{[K^* U_e(\delta^* + \theta)]_u + [K^* U_e(\delta^* + \theta)]_l\} \quad (10)$$

To introduce curvature effects using the second approach for the viscous/inviscid matching condition, the flux expressions

Table 1 Loads, RAE2822 Airfoil: $M_\infty = 0.676$, $Re = 5.7 \times 10^6$

	α	C_l	C_d	$C_{d\infty}$
Experiment	2.40	0.5660	0.0085	—
Corrected exp.	1.93	0.5660	0.0085	—
Inviscid	1.93	0.7290	0.0000	—
Viscous	1.93	0.5835	0.0074	0.0098
Less curvature	1.93	0.5804	0.0074	0.0098
Less wake	1.93	0.5685	0.0059	—

Table 2 Loads, RAE2822 Airfoil: $M_\infty = 0.734$, $Re = 6.5 \times 10^6$

	α	C_l	C_d
Experiment	3.19	0.8030	0.0168
Corrected exp.	2.78	0.8030	0.0168
Inviscid	2.78	1.0122	0.0252
Viscous	2.78	0.7997	0.0179
Less curvature	2.78	0.7907	0.0174
Less wake	2.78	0.7405	0.0126

Table 3 Loads, RAE2822 Airfoil: $M_\infty = 0.75$, $Re = 6.2 \times 10^6$

	Grid[a]	α	C_l	C_d
Experiment	—	3.19	0.7430	0.0242
Corrected exp.	—	2.81	0.7430	0.0242
Inviscid	—	2.81	1.0362	0.0392
Viscous	C.M.	2.81	0.7372	0.0217
Viscous	A.W.	2.81	0.7620	0.0229
Less curvature	C.M.	2.81	0.7466	0.0220
Less curvature	A.W.	2.81	0.7404	0.0239
Less Wake	C.M.	2.81	0.6558	0.0132

[a]A.W. = adapted wake, C.M. = conformal mapping.

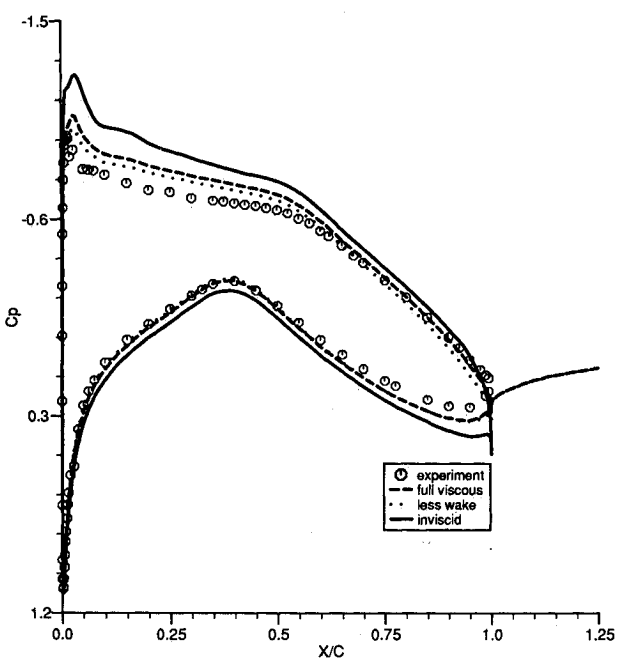

Fig. 2 C_p distribution on the RAE 2822 airfoil: $M = 0.676$, $\alpha = 2.4$ deg, $Re = 5.7 \times 10^6$.

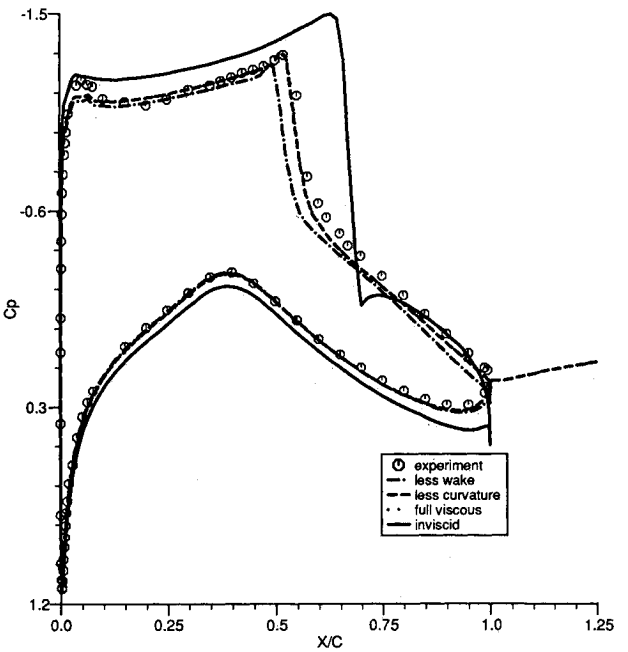

Fig. 3 C_p distribution on the RAE 2822 airfoil: $M = 0.734$, $\alpha = 2.78$ deg, $Re = 6.5 \times 10^6$.

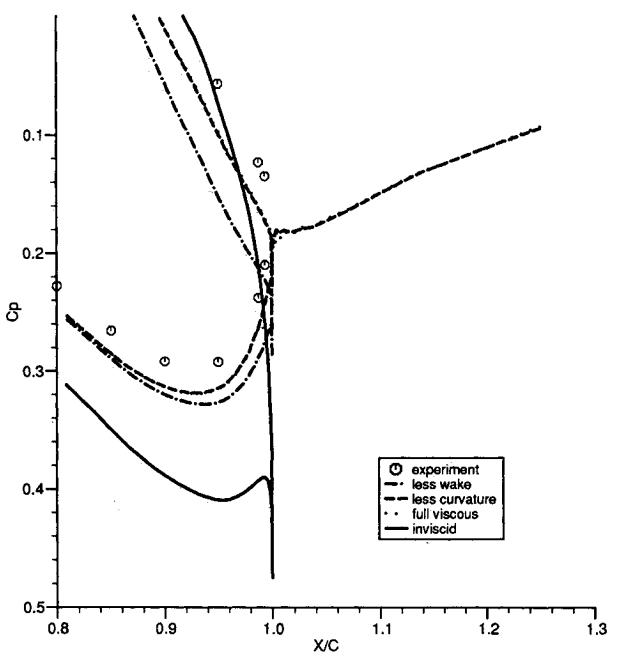

Fig. 4 C_p distribution around trailing-edge region of the RAE 2822 airfoil: $M = 0.734$, $\alpha = 2.78$ deg, $Re = 6.5 \times 10^6$.

do not change except for the Cartesian components of the velocity that are modified in the following way:

$$U_{u,l} = [(U_e)_{u,l} \mp \Delta u/2] \cos \beta_{u,l} - \Delta v \sin \beta_{u,l}$$
$$V_{u,l} = [(U_e)_{u,l} \mp \Delta u/2] \sin \beta_{u,l} + \Delta v \cos \beta_{u,l} \quad (11)$$

To summarize, in the inviscid equivalent flow the viscous effects are simulated on the body through a source distribution whereas on the wake they are simulated through a source/vortex distribution.

Interaction Procedure

The semi-inverse approach proposed by Carter[17] has been used, in which the displacement thickness distribution is updated during the iteration process as follows:

$$\delta^{*n+1} = \omega\left[\delta^{*n}\left(\frac{\tilde{U}_e}{U_e}\right)\right] + (1 - \omega)\delta^{*n} \quad (12)$$

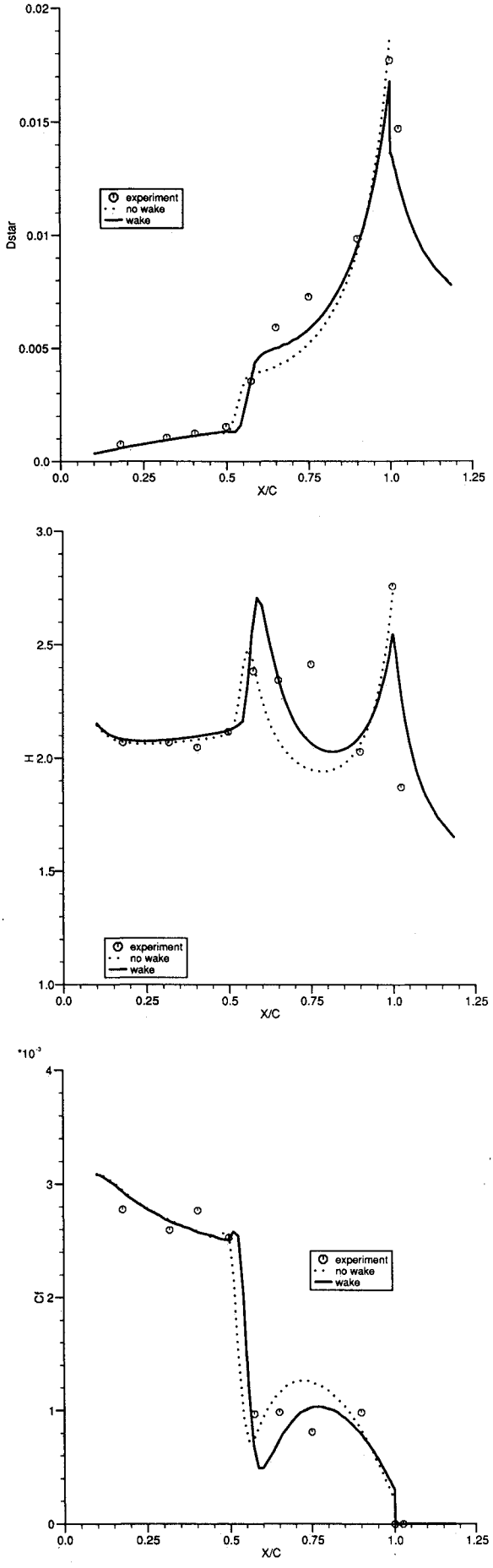

Fig. 5 Boundary-layer parameters for the RAE 2822 airfoil: M = 0.734, α = 2.78 deg, Re = 6.5 × 10⁶.

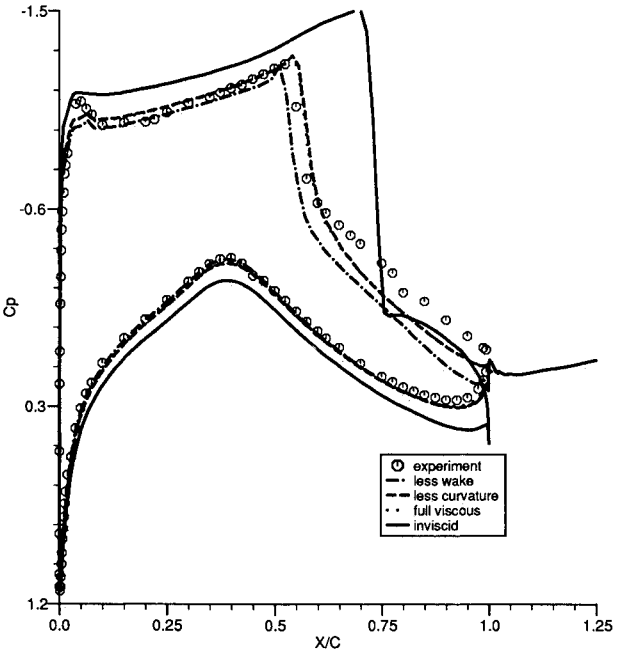

Fig. 6 C_p distribution on the RAE 2822 airfoil: M = 0.75, α = 2.81 deg, Re = 6.2 × 10⁶.

The interaction method proceeds in the following way. The inviscid solution is advanced in time until the aerodynamic global characteristics (e.g., lift coefficient) do not vary significantly and then the boundary-layer calculations are started. The boundary-layer updating occurs every 10 Euler cycles, since this number was found to give the most efficient interaction procedure. In fact, it represents a compromise between the loss of efficiency due to a large number of inviscid cycles between two successive boundary-layer updates and the loss of efficiency caused by increasing the frequency of the boundary-layer computations. The convergence parameter is defined as the ratio $\varepsilon = |(\tilde{U}_e - U_e)/\tilde{U}_e|$, which is a very strict criterion.

Results and Discussion

To test the validity of the present approach for the wake computation, the RAE 2822 airfoil has been chosen. Calculations relative to the test cases 1, 9, and 10 in Ref. 18 have been performed, and results have been compared with experimental data. To understand the influence of the wake on local and global characteristics of airfoils, the viscous terms related to it have been selectively dropped from the computation. To put in evidence the effects due to these terms, C_l and C_d values, obtained using the full viscous model, the full viscous model less wake curvature terms, and the full viscous model less wake terms, are shown in Tables 1, 2, and 3. The corrected angles of attack suggested in Ref. 18 have been used in the computations. The discussion of the three test cases follows.

In the subcritical case 1, the inclusion of the wake computation is significant only for the aerodynamic coefficients. In fact, as can be seen in Fig. 2, the differences between the pressure distributions with and without wake calculations are not so evident. On the contrary, an increment of the C_d values of about 20% and an increment of C_l of about 2% with respect to the case without wake have been obtained (Table 1). In this case, it can also be observed that the wake curvature contribution has almost no effect on global characteristics. This is probably due to the small angle of attack considered and therefore to the small curvature of the wake. The value of $C_{d\infty}$, the profile drag determined from the momentum thickness evaluated at the end of the wake ($C_{d\infty} = 2\theta_\infty$), is also shown in Table 1. The difference between $C_{d\infty}$ and C_d, obtained by integrating pressure plus skin friction, can be con-

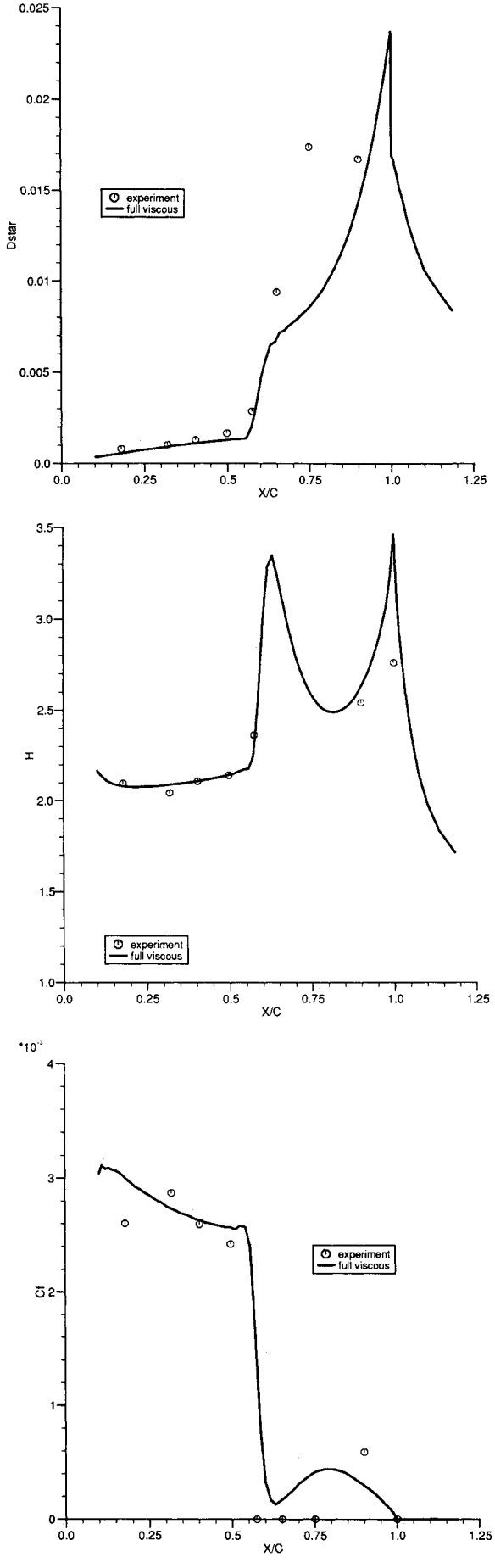

Fig. 7 Boundary layer parameters for the RAE 2822 airfoil M = 0.75, α = 2.81 deg, Re = 6.2 × 10^6.

sidered a measure both of the adequacy of the theoretical model and of the quality of the computations. The reason for the disagreement shown in Table 1 is under investigation. It is believed at this point to be caused by the shortness of the wake and by the lack of any kind of extrapolation of θ to its asymptotic value.

In the supercritical test case 9, the comparison between the approaches previously discussed for computing matching conditions has been performed. It has been found that the values of the global aerodynamic coefficients in the two cases almost coincide. Figures 3 and 4 show that in this case the wake computation leads to some remarkable differences also in the pressure distribution. In particular, the wake reduces the pressure at the trailing edge causing the shock to move a little downstream. In Figure 5, the boundary-layer parameters for the calculations with and without wake are reported together with experimental data. The inclusion of the wake in the viscous model leads to better agreement with experiments, especially in the aft-shock region. In any case, the influence on the aerodynamic coefficients is still the most evident. In fact, the increment of C_d and C_l is, respectively, about 40 and 8%, as shown in Table 2.

The same wake effects have been found in the supercritical test case 10. In Figure 6, the comparison between pressure distributions obtained using the previously described viscous models and experimental data is reported. Even in this case the inclusion of the wake leads to a better prediction of the shock location and pressure distribution in the trailing-edge region. In Figure 7, the boundary-layer parameters are reported; the disagreement with experimental data is due to the lack of the shock-induced separation, not predicted by the calculations.

The influence of the shape of the wake dividing streamline has been checked by means of two different approaches for the construction of the trailing-edge grid line, as described above. The numerical results obtained with the two approaches show a little dependency on the wake geometry, as shown in Table 3. However, it can be concluded that the computational effort needed to generate a grid imposing the trailing-edge line to be a streamline is not justified by the results, at least in the low-incidence transonic cases examined. Furthermore, because the gradients occurring in the trailing-edge region are very strong, careful attention has to be devoted to the distribution of points to ensure the stability and accuracy of the methods. In fact, the C_d value is highly sensitive to the criterion chosen to cluster points in the vicinity of the trailing edge.

Concluding Remarks

The extension of previous work by the authors to the computation of the wake using an Euler/boundary-layer coupling technique has been presented. Both wake displacement and curvature effects have been considered. Two different ways of computing matching conditions in the wake have been described: numerical tests have shown no significant difference. The inclusion of the wake has led to a significant improvement in the prediction of the aerodynamic forces, in particular drag. Some dependence on the wake geometry for the tested transonic cases has been found. Furthermore, high sensitivity of the C_d values to the point distribution has been experienced. The application of the wake calculation described to multicomponent airfoils is under study.

References

[1]Lock, R. C., and Fermin, M. P. C., "Survey of Techniques for Estimating Viscous Effects in External Aerodynamics," *Numerical Methods in Aeronautical Fluid Dynamics*, edited by P. L. Roe, Academic, New York, 1982, pp. 337–430.

[2]Melnik, R. E., Chow, R. R., Mead, H. R., and Jameson, A., "An Improved Viscid/Inviscid Interaction Procedure for Transonic Flow Over Airfoils," NASA CR-3805, Oct. 1985.

[3]Drela, M., "Newton Solution of Coupled Viscous/Inviscid Mul-

tielement Airfoil Flows," AIAA Paper 90-1470, June 1990.

[4]Coiro, D. P., Amato, M., and de Matteis, P., "Numerical Prediction of Transonic Viscous Flows Around Airfoils Through an Euler/Boundary Layer Interaction Method," AIAA Paper 90-1537, June 1990.

[5]Lighthill, M. J., "On Displacement Thickness," *Journal of Fluid Mechanics,* Vol. 4, Pt. 4, 1958, pp. 661–663.

[6]Jameson, A., Schmidt, W., and Turkel, E., "Numerical Solution of the Euler Equations by Finite Volume Methods Using Runge-Kutta Time-Stepping Schemes," AIAA Paper 81-1259, June 1981.

[7]de Matteis, P., "Metodi Multigrid in Fluidodinamica Computazionale," Tesi di Laurea, Istituto di Aerodinamica, Università degli Studi di Napoli, Naples, Italy, 1988.

[8]Rizzi, A., "Numerical Implementation of Solid-Body Boundary Conditions for the Euler Equations," *Zeitschrift für Angewandte Mathematik und Mechanik,* Vol. 58, 1978, pp. T301-T304.

[9]Coiro, D. P., "Metodi Integrali di Strato Limite Inverso e Applicazioni Numeriche," Tesi di Laurea, Istituto di Gasdinamica, Università degli Studi di Napoli, Naples, Italy, 1985.

[10]Whitfield, D.L., Swafford, T. W., and Jacocks, J. L., "Calculation of Turbulent Boundary Layers with Separation and Viscous-Inviscid Interaction," *AIAA Journal,* Vol. 19, No. 10, 1981, pp. 1315–1322.

[11]Coiro, D. P., de Matteis, P., and Amato, M., "An Euler/Boundary Layer Interaction Method for Transonic Flow Calculations Around Airfoils," *Proceedings of the 10th A.I.D.A.A. Conference,* ETS Editrice, Pisa, Italy, Oct. 1989, pp. 23–31.

[12]Green, J. E., Weeks, D. J., and Broman, J. W. F., "Prediction of Turbulent Boundary Layers and Wakes in Compressible Flow by a Lag-Entrainment Method," R.A.E. TR 72231, 1972.

[13]Lock, R. C., "Calculation of Viscous Effects on Aerofoils in Compressible Flow," Royal Aircraft Establishment, RAE TM-AERO-1646, Farnborough, England, Sept. 1975.

[14]Amato, M., "Scelta Ottimale del Grigliato in Aerodinamica," Tesi di Laurea, Istituto di Aerodinamica, Università degli Studi di Napoli, Naples, Italy, 1988.

[15]Johnston, W., and Sockol, P., "Matching Procedure for Viscous-Inviscid Interactive Calculations," *AIAA Journal,* Vol. 17, No. 6, 1979, pp. 661–663.

[16]Thomas, J. L., "Transonic Viscous-Inviscid Interaction using Euler and Inverse Boundary Layer Equations," Ph.D. Thesis, Mississippi State University, Mississippi State, MS, 1983.

[17]Carter, J. E., "A New Boundary Layer Inviscid Interaction Technique for Separated Flows," AIAA Paper 79-1450, 1979.

[18]Anon., "Experimental Data Base for Computer Program Assessment," AGARD-AR-138, May, 1979.